Sharp line emission of $KZnF_3:Cr^{3+}$

O. Pilla,* P. T. C. Freire,† and V. Lemos
Instituto de Física "Gleb Wataghin," Universidade Estadual de Campinas–UNICAMP, Campinas, São Paulo, 13083-970, Brazil
(Received 24 January 1995)

Emission spectra of $KZnF_3:Cr^{3+}$ obtained at several pressures and temperatures are presented. The results allow for the construction of a Tanabe-Sugano–type diagram illustrating the transition from low- to high-crystal-field regime for cubic and distorted centers. Assignments of sharp lines are given based on the analysis of these diagrams, time-resolved spectroscopy, and lifetime analysis.

I. INTRODUCTION

Several solid-state wide band tunable lasers developed in the past few years stimulated recent basic research.[1–6] The reason for the tunability is that some of the electronic transitions of the impurities are strongly coupled to the lattice of the host crystal and exhibit broad-vibronic emission bands. The laser suitability of single crystals doped with transition-metal ions (TMI) is widely recognized.[7–9] The vibronic laser system $KZnF_3:Cr^{3+}$ is highly adequate due to its excellent optical properties: this is the only TMI laser material for which the emission can be made to occur in the red portion of the visible spectrum by application of small amounts of pressure.[1] The laser gain profile is related to the shape function of the emission spectrum and the peak position of both curves is nearly coincident in this material. The fact is highly significant because of the development of wide band tunable lasers in the visible spectrum at room temperature, and also because of the possibility of selecting the tuning range with available pressures. Therefore, it is fundamental that a complete understanding of emission properties of this material is achieved, including high-crystal-field regions beyond the crossover point where the lowest electronic excited states are degenerated.

In pursuing this purpose in the present investigation luminescence measurements were performed at low temperature and high pressures, allowing for the observation of sharp line spectra. The lines were identified with zero-phonon lines of cubic and lower symmetry centers.

II. EXPERIMENT

The $KZnF_3:Cr^{3+}$ single crystals used in this work were grown by Dürr as described before.[1] The undoped crystals have perovskite structure and the Cr^{3+} ion site symmetry is predominantly cubic ($\sim$ 90%). Distorted centers are present in lower abundance, i.e., $\sim$ 10% for trigonal and <1% for tetragonal site symmetry.[10] The samples prepared for high-pressure experiments were $\cong$ 50 μm slabs cut along a cubic axis. The cell employed was a membrane diamond-anvil cell loaded with Ar.[11] The luminescence of $MgO:V^{2+}$ served the purpose of calibrating the pressure, which included corrections for low-temperature shifts.[12] One of two laser lines was used as excitation: the 514.5 nm line of an Ar ion laser or the 632.8 nm line of a He-Ne laser. Analysis was made with a Spex Triplemate 1877, a Hamamatsu R943-02 photomultiplier, and a photon counting system. For time-resolved spectra and lifetime measurements we used a chopper in the beam and an acoustic-optic modulator.

III. RESULTS AND DISCUSSION

Sharp lines appear in the emission of $KZnF_3:Cr^{3+}$ in the range of high crystal field. Figure 1 shows spectra taken at three different conditions of temperature and fixed pressure, P=11.0 GPa, with excitation line λ = 514.5 nm. At T=180 K, three lines dominate the spectrum. The lines occurring at 14 872 and 14 750 cm^{-1} at this temperature value, labeled S_1 and S_2 in Fig. 1, may

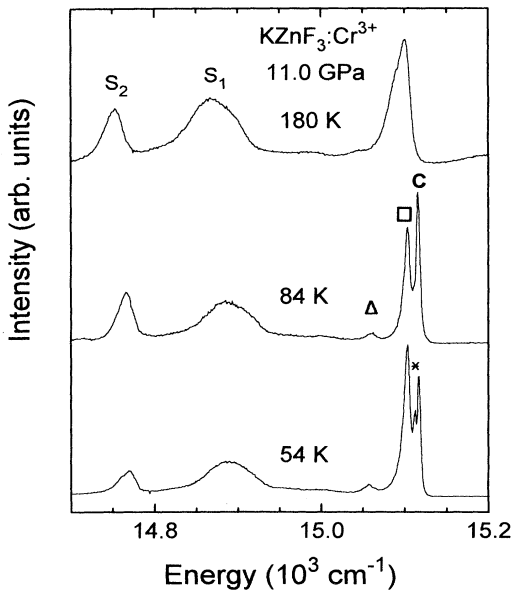

FIG. 1. High-resolution luminescence in the high-crystal-field regime taken with λ_{ex} = 514.5 nm at three temperature values.

be attributed to phonon sidebands. They are due to interaction of electronic states with lattice vibrations of the host crystal. This assignment was based on the following consideration. First of all, a symmetrical set, S_1', S_2' occurs at the high-energy side of the pure electronic line for moderate temperatures ($300 \geq T \geq 150$ K). The lower energy set relative intensities agree with Stokes population factor [see upper curve of Fig. 1, and the anti-Stokes component (not shown in Fig. 1) intensities rate is well described by the Boltzmann population factor. The frequency shifts (average between S_i and S_i')] observed from the zero-phonon line, ZPL, are $\omega_1 = 214$ cm^{-1} and $\omega_2 = 343$ cm^{-1}, respectively. These numbers are close to the frequencies of zone-center phonons determined from infrared studies:[13] $\omega(\mathrm{TO}_2) = 199$ cm^{-1}, $\omega(\mathrm{LO}_2) = 295$ cm^{-1}. Vibrational states due to multiphonon processes also lie in the vicinity of those observed frequencies:[14] $\omega(\mathrm{TA} + \mathrm{TO}_1) = 201$ cm^{-1}, $\omega(\mathrm{TO}_2 + \mathrm{TO}_1) = 330$ cm^{-1}, and $\omega(\mathrm{LO}_2 + \mathrm{TO}_1) = 351$ cm^{-1}. Finally, there are some zone-edge phonons with frequencies around those values.[14] All these phonon modes may possibly couple to the electronic states and give rise to lines S_1 and S_2 in the luminescence spectra. Next we analyze the group of lines around 15 100 cm^{-1} in the spectra shown in Fig. 1. The lines resolve into three peaks at $T = 84$ K, which we label as C, $\square$, and $\triangle$ in the corresponding spectrum of the figure. This labeling was chosen because the cubic, C, tetragonal, $\square$, and trigonal, $\triangle$, ZPL's should occur in accordance with the criteria of higher symmetry centers emitting at higher energies.

Even though the majority of ions Cr^{3+} substitute Zn^{2+} in the O_h site symmetry, the lower symmetry centers contribute to the emission spectra. We point out that in the case of group O_h, the electric dipole operator has odd parity, and electric dipole transitions between states of same parity are forbidden. As the magnetic dipole operator is of even parity, this kind of transition is allowed between same parity states, although through a weaker process than those of electric dipole transitions. The tetragonal C_{4v} and trigonal C_{3v} groups lack inversion symmetry. Hence, in the distorted sites the stronger electric dipole transitions are no longer parity forbidden. This is the reason why, even being less abundant, the tetragonal and trigonal Cr^{3+} give important contribution to the emission spectra. In Fig. 1, the lowest curve illustrates the appearance of a new sharp line on lowering the temperature to $T = 54$ K, marked with an asterisk in the figure. The identification of this line is made easier by constructing energy diagrams. One such diagram, a Tanabe-Sugano-type diagram, is shown in Fig. 2. In this figure we adopted the convention of solid, dotted, and dashed lines to represent the cubic, tetragonal, and trigonal energies, respectively. The lines with nonzero slope are representative of $^4T_2 \longrightarrow ^4A_2$ transition energy behavior, and those parallel to the pressure axes correspond to $^2E \longrightarrow ^4A_2$ transitions. The linear coefficients for $^4T_2$ curves were obtained from previous reported data[1] as well as the slope of 167 cm^{-1}/GPa. The latter was assumed to be the same value for all of the centers. The values of $^2E \longrightarrow ^4A_2$ transition energies were taken from the spectrum of $T = 84$ K and $P =$

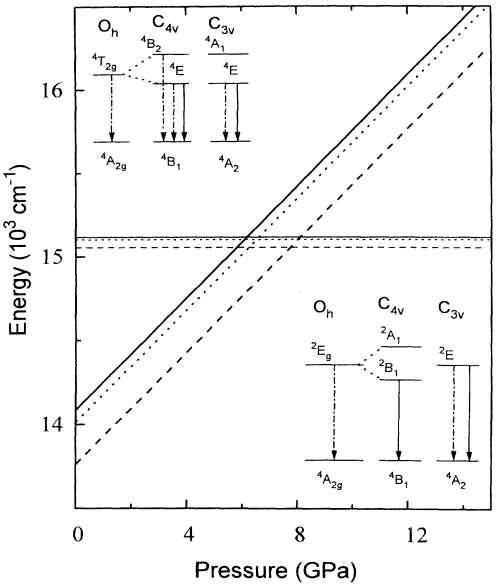

FIG. 2. Dependence of emission energies with pressure, for cubic (solid lines), tetragonal (dotted lines), and trigonal (dashed lines) symmetries. Corresponding energy diagrams are drawn for low- and high-crystal-field, respectively.

11.0 GPa. In the diagram, the states $^4T_2$ and ^2E cross at $P_C = 6.2$ GPa, $P_\square = 6.5$ GPa, and $P_\triangle = 7.7$ GPa. The crossover point defines the transition from low- to high-crystal-field regimes. Even though oversimplified, this diagram helps to describe the otherwise complicated process of transition. Included in the upper left side of the figure are energy-level diagrams for the crystal in the low-crystal-field regime. The counterpart diagram for high crystal field is found at the bottom right side of the figure. The diagrams serve to show the allowed transitions through electric dipole process (full vertical lines) and magnetic dipole process (dashed dotted lines). From these diagrams it is possible to scale the transitions with oscillator strength, qualitatively. The dominant oscillator strengths are related to the triply allowed (spin, electric dipole, and magnetic dipole) transitions in the low-crystal-field regime. This is the case of $^4E \longrightarrow ^4B_1$ transitions in C_{4v} and $^4E \longrightarrow ^4A_2$ transitions in C_{3v} group. The intermediate oscillator strengths are provided by the spin-forbidden transitions $^2B_1 \longrightarrow ^4B_1$ of C_{4v} and $^2E \longrightarrow ^4A_2$ of C_{3v} in the high-crystal-field regime. The weaker oscillator strengths are those of the electric dipole forbidden transitions of O_h group. Keeping this scaling in mind it is possible to interpret the lines in Fig. 1 by identifying them with the diagrams of Fig. 2. The results are shown in Table I. It is worthwhile mentioning that in the high-crystal-field regime the $^2B_1$ state is a singlet and that there is no allowed transition from the singlet $^2A_1$ to the ground state. As a consequence, the tetragonal centers emit only one line (identified in Table I). The line labeled asterisk should not occur as a result of tetragonal center emission. It is probably due to the lower energy member of the doublet ^2E_g. In a first approximation it is degenerate, but the combined effect of spin-orbit coupling and axial field splits the ^2E_g state

TABLE I. Position and linewidth of sharp lines and their identification according to the energy diagrams of Fig. 2.

Symbol [P(GPa)/T(K)]	$\omega(cm^{-1})$	$\Gamma(cm^{-1})$ [11.0/54]	Transition	$\omega(cm^{-1})$	$\Gamma(cm^{-1})$ [8.5/25]	Transition
C	15 117	3	$^2E_g \longrightarrow {}^4A_{2g}$	15 118	5	$(^2E_g \longrightarrow {}^4A_{2g}) + {}^4T_{2g} \longrightarrow {}^4A_{2g}$
*	15 112	5	$^2E_g \longrightarrow {}^4A_{2g}$			
□	15 103	7	$^2B_1 \longrightarrow {}^4B_1$	15 106	12	$(^2B_1 \longrightarrow {}^4B_1) + (^4E \longrightarrow {}^4B_1)$
△	15 057	16	$^2E \longrightarrow {}^4A_2$	15 073	42	$(^2E \longrightarrow {}^4A_2) + (^4E \longrightarrow {}^4A_2)$

into two Kramers doublets as in the case of the R_1 and R_2 lines of ruby.[15] Because of strong temperature decrease of the ratio I_C/I_* in the cryogenic region,[16] the asterisk line is revealed when temperature drops to 54 K.

At higher pressures, $P \gg 7.7$ GPa, the electronic states are well separated and the interpretation of line spectra in terms of isolated ^2E and $^4T_2$ states is meaningful. When the states are close enough in energy they may interact and the luminescence spectra reflect a superposition of the properties of these states. The concurrence of mixing of states through spin-orbit coupling,[17] apart from thermal population effects, adds complexity to the problem and just a qualitative description will be attempted here. We notice that the close proximity of the states ^2E and $^4T_2$ produces broadening and changes in position. In Fig. 3 spectra at a fixed pressure and three very close temperature values are presented. One observes first that the cubic line is unique even at the lowest temperature value (T = 25 K) at P= 8.5 GPa, in contrast with the breakdown of degeneracy of ^2E_g lines shown in the 54 K spectrum of Fig. 1. It was also observed that this line shifts towards higher energy on lowering the temperature

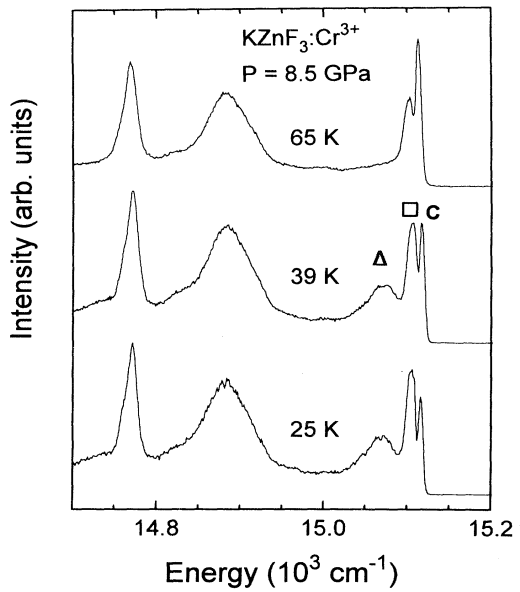

FIG. 3. High-resolution luminescence spectra taken close to the crossing from low- to high-crystal-field region with λ_{ex} = 632.8 nm at three temperature values.

from 65 to 25 K. This is surprising in the light of the behavior of electronic levels which have negligible displacements with temperature below 90 K in high-crystal-field $3d^3$ systems.[18]

The spectrum represented in the lowest curve of Fig. 3 gave the results for the energies and linewidths also listed in Table I. It is possible to see in this table that the positions of the lines □ and Δ are considerably changed with respect to their 11.0 GPa values. This is completely unexpected based on our simplified model giving zero slope for the $^2E_g \longrightarrow {}^4A_{2g}$ transition energies with pressure.

Finally, severe broadenings are observed to occur for all ^2E_g lines at 8.5 GPa as compared with higher pressure values (see Table I). Nonhydrostaticity conditions should not be attempted to justify these broadenings because linewidths are bigger at the lower pressure value. Also, populational effects should be discarded because the lines are broader at T= 25 K than at T = 54 K. These effects are probably a result of the mixing of electronic states $^4T_2$ and ^2E_g due to the close proximity of the crossing from low- to high-crystal-field region. The mixing of such states has been considered previously[18] with a configurational-coordinate model in the harmonic approximation to describe the vibrational states of small $^4T_2$-^2E_g energy separation Δ in $3d^3$-ion systems. In this model, the mixing is expressed as a superposition of electronic-vibrational wave functions and the spin-orbit operator is adopted as the interaction operator. The calculated zero-vibrational states energy plots show marked variations with temperature in the case of very small Δ. Their calculation also shows that broadening of R lines with temperature should be larger in smaller Δ systems. Their findings indicate that the anomalous spectral properties of $KZnF_3:Cr^{3+}$ at P = 8.5 GPa described above should be attributed to mixing of states effect. The degree of mixing could be described by an analogous model. The specific case of this material is complicated by the need to consider the wave functions of cubic and distorted centers.

For the sake of completeness we add that the relative intensities of ^2E_g lines was observed to vary according to the fact that population of the upper levels diminish on lowering the temperature, for both pressure values 8.5 and 11.0 GPa.

In spite of this mixture, it is still possible to distinguish the trigonally distorted centers emission. Their lifetime is $\sim$ 300 μs whereas the emissions from cubic

and tetragonal centers have a long lifetime ($\sim$ 4 ms).[19] That is the reason why we performed time-resolved measurements and the results are given in Fig. 4. The spectra were taken with $\lambda_{ex} = 632.8$ nm to favor distorted center emission. In this figure, curve (a) corresponds to the total emission. The frequency span from 13.5×10^3 cm^{-1} to 15.5×10^3 cm^{-1}. In this wide range the resolution employed did not allow the separation of the peaks arising from cubic centers from the tetragonal ones. The peak labeled $\square + C$ in Fig. 4 represents the unresolved components. The intermediate curve (b) is the spectrum of slow electronic transitions ($\tau \sim 2$ ms). It contains contributions from tetragonal and cubic site symmetries, but rules out any component of trigonal centers. It is noticeable in (b) the disappearing of the peak labeled $\triangle$ in (a) and of the broadband emission centered at about 14 300 cm^{-1}. Curve (c) is the difference between (a) and (b). Being the fast emission, it selects the pure trigonally distorted contribution from the others. It contains the ZPL, the highest-energy line, and two phonon bands at the lower-energy side, corresponding to S_1 and S_2 of the total emission, respectively. Also present is a broadband which is due to a multiphonon sideband of the ZPL. The presence of both the broadband multiphonon and sharp line emission with comparable intensities is another evidence of the mixing of states effect. In fact, the trigonal crossover point P_Δ is the closest to pressure analyzed here, 8.5 GPa, and the trigonal lines the most affected accordingly (see Table I).

The inset of Fig. 4 is the high-resolution luminescence with total emission (solid line) and the slow component (dotted line). In the frequency range of ZPL's the dominant contribution arises from tetragonal centers. The positions marked by arrows correspond to trigonal emission. It is noticeable that the two lower-energy arrows are distant from the first, by the same amount as S_1 and S_2 differ from the cubic ZPL. This fact reinforces the interpretation of the vibrational origin of these lines.

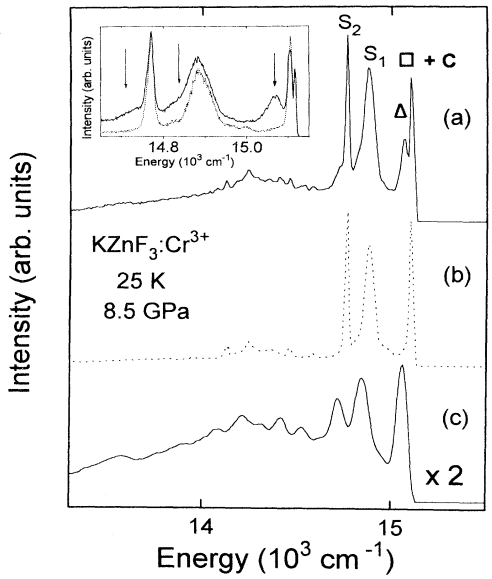

FIG. 4. Time resolved spectra for (a) total emission, (b) slow component ($\tau \sim 2$ ms), and (c) difference between spectra (a) and (b) giving the fast component of emission.

IV. CONCLUSION

High-resolution luminescence measurements were performed in an interesting system with several distorted site symmetries. First hand identification of sharp lines due to pure electronic transitions is provided. Time-resolved spectroscopy results support the identification. Additional features in the fast component spectra are interpreted in terms of phonon sidebands, in comparison with the cubic center emission. Broadenings and line displacements observed close to the crossing from low- to high-field region were attributed to mixing of states effect.

ACKNOWLEDGMENTS

Financial support from Conselho Nacional de Desenvolvimento Científico e Tecnológico (CNPq), Fundação de Amparo à Pesquisa do Estado de São Paulo (FAPESP), Fundo de Apoio ao Ensino e à Pesquisa (FAEP/UNICAMP) and Consiglio Nazionale delle Ricerche (CNR) are greatly acknowledged.

* Permanent address: Dipartimento di Fisica, Università degli Studi di Trento, 38050, Povo-Trento, Italy.
† Permanent address: Departamento de Física, Universidade Federal do Ceará, 60455-760, Fortaleza, Brazil.

[1] P.T.C. Freire, O. Pilla, and V. Lemos, Phys. Rev. B **49**, 9232 (1994).
[2] H. Eilers, U. Hömmerich, S.M. Jacobsen, W.M. Yen, K.R. Hoffman, and W. Jia, Phys. Rev. B **49**, 15 505 (1994).
[3] H. Manaa, Y. Guyot, and R. Moncorge, Phys. Rev. B **48**, 3633 (1993).
[4] M. Grinberg, A. Brenior, G. Boulon, C. Pedrini, and C. Madej, J. Lumin. **55**, 303 (1993).
[5] J.F. Donegan, G.P. Morgan, T.J. Glynn, and G. Walker, J. Mod. Opt. **37**, 769 (1990).
[6] Z. Zhang, K.T.V. Grattan, and A.W. Palmer, Phys. Rev. B **48**, 7772 (1993).
[7] B. Henderson and G.F. Imbusch, Comtemp. Phys. **29**, 235 (1988).
[8] U. Dürr, U. Brauch, W. Knierin, and C. Schiller, in *Tunable Solid State Lasers*, edited by P. Hammerling, A.B. Bugdor, and A. Pinto (Springer-Verlag, Berlin, 1985).
[9] U. Dürr and U. Brauch, in *Tunable Solid State Lasers II*, edited by A.B. Bugdor, L. Esterowitz, and L.G. Deghazer (Springer-Verlag, Berlin, 1986).
[10] U. Brauch and U. Dürr, Opt. Commun. **49**, 61 (1984).
[11] R. Letoullec, J.P. Pinceaux, and P. Loubeyre, in *High Pressure Science and Technology*, edited by M. Ross (Gordon and Breach, London, 1990), Vol. 5, p. 871.
[12] B. di Bartolo and R. Peccei, Phys. Rev. **137**, A1770 (1965).
[13] C.H. Perry and E.F. Young, J. Appl. Phys. **38**, 4616 (1967).
[14] E.F. Young and C.H. Perry, J. Appl. Phys. **38**, 4628 (1967).
[15] S. Sugano and M. Peter, Phys. Rev. B **122**, 381 (1961).
[16] B.A. Weinstein, Rev. Sci. Instrum. **57**, 910 (1986).
[17] C.J. Donnelly, T.J. Glynn, G.P. Morgan, and G.F. Imbusch, J. Lumin. **48&49**, 283 (1991).
[18] C.J. Donnelly, S.M. Healy, T.J. Glynn, G.F. Imbusch, and G.P. Morgan, J. Lumin. **42**, 119 (1988).
[19] O. Pilla, E. Galvanetto, M. Montagna, and G. Viliani, Phys. Rev. B **38**, 3477 (1988).